Electromagnetic waves in a strong Schwarzschild plasma

James Daniel and Toshiki Tajima
Department of Physics and Institute for Fusion Studies, The University of Texas at Austin, Austin, Texas 78712
(Received 5 November 1996)

The physics of high-frequency electromagnetic waves in a general relativistic plasma with the Schwarzschild metric is studied. Based on the $3+1$ formalism, we conformalize Maxwell's equations. The derived dispersion relations for waves in the plasma contain the lapse function in the plasma parameters such as in the plasma frequency and cyclotron frequency, but otherwise look ''flat.'' Because of this property this formulation is ideal for nonlinear self-consistent particle [particle-in-cell (PIC)] simulation. Some of the physical consequences arising from the general relativistic lapse function as well as from the effects specific to the plasma background distribution (such as density and magnetic field) give rise to nonuniform wave equations and their associated phenomena, such as wave resonance, cutoff, and mode conversion. These phenomena are expected to characterize the spectroscopy of radiation emitted by the plasma around the black hole. PIC simulation results of electron-positron plasma are also presented. [S0556-2821(97)07108-7]

PACS number(s): 52.60.+h, 52.65.−y, 52.65.Rr

I. INTRODUCTION

There is ample evidence that a black hole is involved in a variety of astrophysical phenomena such as γ-ray bursts [1] and active galactic nuclei (AGN) jets [2]. Yet plasma physics in a fully general relativistic framework is in its infancy, mainly in a cosmological metric [3,4] and quite recently a magnetohydrodynamic study [5,6]. Here we are interested to start looking into the spectroscopic signatures of radiation emitted from a plasma around a black hole. It has been known [7] that corpuscular orbits are unstable within three Schwarzschild radii (R_S). Because of this, it has been generally believed that no plasma is present within $3R_S$. Recently, however, we have demonstrated [6] that the (collisional) gas dynamics is different from the corpuscular orbital dynamics and thus that magnetohydrodynamic equilibria that hold plasma between the horizon ($1R_S$) and $3R_S$ (as well as beyond) do exist. It is here that strong general relativistic plasma effects are particularly severe and that perturbative post-Newtonian approaches [8] are inadequate.

MacDonald and Thorne [9,10] have introduced Maxwell's equations in $3+1$ coordinates, which provides a foundation for formulation of a general relativistic (GR) set of plasma physics equations. In Sec. II, we conformalize this $3+1$ set of equations, so that they can be transformed into terms completely analogous to Maxwell's equations. In Sec. III, the transformations which compose the conformalization are used to write the dispersion relation for positron-electron plasma in new terms. Section IV discusses resonance and cutoff points, applying the results of Secs. II and III to show the effect of a strong gravitational field on the plasma properties. A $1\frac{2}{2}$-dimensional particle simulation is also employed to demonstrate the model, and offers unforeseen results when applied to mode conversion. A discussion and summary are given in Sec. V.

II. CONFORMALIZING MAXWELL'S EQUATIONS

A. Derivation of the conformalism

The following summarizes how to conformalize Maxwell's equations from a $3+1$ Schwarzschild metric. Thorne, Price, and McDonald [10] have given the $3+1$ solution for Maxwell's equations in the Schwarzschild metric:

$$\nabla\cdot\vec{E}=4\pi\rho, \tag{1}$$

$$\nabla\cdot\vec{B}=0, \tag{2}$$

$$\frac{1}{c}\frac{\partial}{\partial t}\vec{E}=\nabla\times(\alpha\vec{B})-4\pi\alpha\vec{J}, \tag{3}$$

$$\frac{1}{c}\frac{\partial}{\partial t}\vec{B}=-\nabla\times(\alpha\vec{E}), \tag{4}$$

$$\frac{d}{d\tau}\vec{p}=q\left(\vec{E}+\frac{\vec{v}\times\vec{B}}{c}\right), \tag{5}$$

where the lapse function α signifies the general relativistic effect around a Schwarzschild black hole,

$$\alpha=\sqrt{1-\frac{R_S}{r}}, \tag{6}$$

the time derivative in Eq. (5) is defined as

$$\frac{d}{d\tau}\equiv\left(\frac{1}{\alpha}\frac{\partial}{\partial t}+\vec{v}\cdot\nabla\right), \tag{7}$$

and R_S is the Schwarzschild radius. All quantities are measured by a local fiducial observer (FIDO). Thus the vector quantities given are neither covariant nor contravariant. The four-metric of our coordinates is

$$ds^2=-\alpha^2c^2dt^2+\alpha^{-2}dr^2+r^2(d\theta^2+\sin^2\theta\, d\phi^2). \tag{8}$$

We shall consider wave propagation in the $\pm\hat{r}$ direction. The ϕ component of $\nabla\times\vec{E}$ is

$$\nabla\times(\alpha E^{\hat{\theta}}\hat{\theta})=\frac{\alpha}{r}\frac{\partial}{\partial r}(r\alpha E^{\hat{\theta}})\hat{\phi}. \tag{9}$$

We can combine this with the wave equation

$$\frac{1}{c^2}\frac{\partial^2}{\partial t^2}\vec{E}=-\nabla\times[\alpha\nabla\times(\alpha\vec{E})]-\frac{4\pi\alpha}{c}\frac{\partial}{\partial t}\vec{J} \tag{10}$$

and, for the moment, allow $\vec{J}=0$. The resulting wave equation is

$$\frac{1}{c^2}\frac{\partial^2}{\partial t^2}E^{\hat{\theta}}=\frac{\alpha}{r}\frac{\partial}{\partial r}\left[\alpha^2\frac{\partial}{\partial r}(\alpha r E^{\hat{\theta}})\right]. \tag{11}$$

Let us make the substitution

$$E_{\xi}^{\hat{\theta}}=\alpha r E^{\hat{\theta}} \tag{12}$$

and change the coordinate variable to ξ, where

$$\frac{\partial}{\partial\xi}=\alpha^2\frac{\partial}{\partial r}. \tag{13}$$

This allows us to rewrite the wave equation as

$$\frac{1}{c^2}\frac{\partial^2}{\partial t^2}E_{\xi}^{\hat{\theta}}=\frac{\partial^2}{\partial\xi^2}E_{\xi}^{\hat{\theta}}. \tag{14}$$

The $3+1$ equations derived by [9] already account for the universal t coordinates, leaving only the three-metric

$$ds^2=\alpha^{-2}dr^2+r^2d\theta^2+r^2\sin^2\theta\,d\phi^2. \tag{15}$$

The curl and divergence operators in the $3+1$ set of equations are covariant and can be derived from the three-metric. Instead of the spherical Scharzchild three-metric, we will employ a ‘‘slab’’ version, which eliminates spherically symmetric artifacts of having chosen to consider propagation along the radial direction. The purpose of choosing such a metric is to isolate the effect of the gravitational field from the choice of spherical coordinates. In the absence of a gravitational field, Eq. (12) would read as $E_{\xi}^{\hat{\theta}}=rE^{\hat{\theta}}$, and the spherical boundary conditions would impose effects on the propagation of the waves, such as cutoffs not unlike those discussed in Sec. IV C. The slab approximation instead defines a plane wave which happens to be traveling in a radial direction and does not ‘‘feel’’ the spherical boundary conditions. Far from the event horizon, the approximation breaks down, since any initial disturbance will propagate according to Huygen’s principle. This does not significantly weaken our approach, however, because there is a qualitative difference in our results only with respect to the idealized cases near the hole discussed in Secs. IV B and IV C, where we wish to demonstrate the part of gravity in creating new cutoffs and resonances. In Sec. IV D and IV E, we can employ either a slab or spherical metric and obtain the same qualitative results, since the background magnetic field and density decrease exponentially, overshadowing the effect of spherical symmetry on the conformalized versions of these fields. Also, the only waves that reach a distant observer are vacuum-propagating light waves (emitted from near the black hole), and the effects of the plasma and the strong gravitational field have already left their signature before a signal is very far from the hole.

By making the substitutions

$$\varrho\equiv r-R_S\ll R_S, \tag{16}$$

$$\partial\theta=\theta-\theta_0\ll\theta_0, \tag{17}$$

$$\partial\phi=\phi-\phi_0\ll\phi_0, \tag{18}$$

$$dy^2=R_S^2d\theta^2, \tag{19}$$

$$dz^2=R_S^2\sin^2\theta_0 d\phi^2, \tag{20}$$

we have chosen a local set of nearly Cartesian (except for ϱ) coordinates, which has the metric

$$ds^2=\alpha^{-2}d\varrho^2+dy^2+dz^2. \tag{21}$$

From the definition in Eq. (16), $d\varrho=dr$, and so the differential equation between ϱ and ξ is the same as that between r and ξ:

$$\alpha^{-2}(\varrho)d\varrho=d\xi, \tag{22}$$

the solution to which is

$$\xi=\varrho+R_S\ln(\varrho)+\text{const}. \tag{23}$$

This changes the wave equation (11) to

$$\frac{1}{c^2}\frac{\partial^2}{\partial t^2}E^{\hat{\theta}}=\frac{\alpha}{R_S}\frac{\partial}{\partial\varrho}\left[\alpha^2\frac{\partial}{\partial\varrho}(\alpha R_S E^{\hat{\theta}})\right], \tag{24}$$

and instead of the substitution Eq. (12), we use the substitution

$$E_{\xi}^{\hat{\theta}}=\alpha E^{\hat{\theta}} \tag{25}$$

to arrive at Eq. (14), since the R_S cancels out. Note that the change in coordinates as stated in Eq. (13) remains the same. The only alteration is in the change in amplitude of the waves, which will now only occur in the presence of a gravitational field, and not because of a particular $r=0$ choice in coordinates.

The three-metric in the conformalized space is

$$ds^2=\alpha^2d\xi^2+dy^2+dz^2. \tag{26}$$

With the substitutions

$$\rho_\xi = \alpha^2 \rho, \tag{27}$$

$$\vec{E}_\xi = \alpha \vec{E}, \tag{28}$$

$$\vec{B}_\xi = \alpha \vec{B}, \tag{29}$$

and

$$\vec{J}_\xi = \alpha^2 \vec{J}, \tag{30}$$

Maxwell's equation become

$$\nabla \cdot \vec{E}_\xi = 4\pi \rho_\xi, \tag{31}$$

$$\nabla \cdot \vec{B}_\xi = 0, \tag{32}$$

$$\frac{1}{c}\frac{\partial}{\partial t}\vec{E}_\xi = \nabla \times \vec{B}_\xi - 4\pi \vec{J}_\xi, \tag{33}$$

$$\frac{1}{c}\frac{\partial}{\partial t}\vec{B}_\xi = -\nabla \times \vec{E}_\xi, \tag{34}$$

with the equation of motion

$$\frac{d}{dt}\vec{p} = q\left(\vec{E}_\xi + \frac{\vec{v}\times\vec{B}_\xi}{c}\right). \tag{35}$$

Momentum and velocity remain unchanged by the conformalism.

These equations are entirely ''flat'': There are no covariant derivatives, and time flows at the same rate regardless of location. The substitutions of Eqs. (27)–(30) map the local quantity to the conformalized ''ξ-space'' quantity, and Eq. (23) maps the radial coordinate to the conformalized ξ coordinate. Given a plasma in a Schwarzschild metric, properties can be mapped to the conformalized space, solved without general relativistic equations, and mapped back into ''real'' space.

B. Frequency in the conformalism and observable phenomena

One concern of using the conformalized set of equations is keeping track of how they relate to the real physics that might be observed far from the hole. As $r \to \infty$, $\alpha \to 1$, and so the local physics far from the hole is ''flat'' and the time far from the hole is universal time. The conformalized ξ-space physics is the same far from the hole as the local physics far from the hole. If we model, for example, some phenomena occurring near the hole from which is emitted some observable electromagnetic wave that propagates far from the hole, the frequency in the model is the same as that which would be observed. The main concern is dealing with the proper time τ of the phenomenon near the hole, where the effects of time dilation are significant. Since $d\tau = \alpha dt$, then $\omega_\tau = \alpha^{-1}\omega_t$, where ω_τ is the locally measured frequency and ω_t is the frequency measured in ξ space as well as the frequency measured far from the hole. The proper time becomes important when there are physically known frequencies, such as that of electron-positron annihilation, which must be translated into universal time.

III. DISPERSION RELATION

The properties of wave propagation are characterized by the dispersion relation. The dispersion relation may be derived by linearizing the Maxwell equations [Eqs. (31)–(34)] and the equation of motion [Eq. (35)] along with the conformalized charge density and current [Eqs. (27) and (30)]. In such a treatment, the dispersion relation is a function of two parameters that can change with respect to position. The conformalized local plasma frequency depends on the local number density of electrons and also upon the local value of the lapse function α:

$$\omega_p = \sqrt{\frac{4\pi\alpha^2[r(\xi)]n_0[r(\xi)]e^2}{m}}. \tag{36}$$

Similarly, the conformalized local cyclotron frequency depends upon both the local magnetic field and the lapse function:

$$\Omega_e = \frac{e\alpha[r(\xi)]B_0[r(\xi)]}{mc}, \tag{37}$$

where $r(\xi)$ is the inverse of $\xi(r) = r - R_S + R_S \ln(r)$.

In the conformalized coordinates and variables, therefore, we have a variation in the cyclotron and plasma frequencies entirely due to the presence of the Schwarzschild metric. Even if the background density and magnetic field were constant with respect to position, the metric would still cause the conformalized cyclotron and plasma frequencies to vary with position. New resonances and cutoffs can appear in the plasma by introducing a strong gravitational field.

High frequency electromagnetic waves in a nonuniform plasma (i.e., ξ-dependent ω_p and Ω_e) can be characterized by a local dispersion relation in the WKB sense. The wave vector is chosen to be $\vec{k} = k\hat{\xi}$, and the background magnetic field is $\vec{B}_0 = B_0 \cos\theta\hat{\xi} + B_0 \sin\theta\hat{z}$, where θ is the angle between the $\vec{B}_0$ and $\vec{k}$. The dispersion relation for the transverse EM wave in an electron-ion plasma is given locally in ξ space as

$$n^2 = \frac{c^2k^2}{\omega^2} = \epsilon(k,\omega) = 1 - \sum_j \frac{\omega_{pj}^2}{\omega^2}\left(1 - \frac{\Omega_j^2\cos^2\theta}{\omega^2} - \frac{\Omega_j^2\sin^2\theta}{\omega^2 - c_{sj}^2k^2}\right)^{-1} \tag{38}$$

for $\vec{E}_1 = E_1\hat{y}$, $\vec{B}_1 = B_1\hat{z}$ polarity and

$$n^2 = 1 - \sum_j \frac{\omega_{pj}^2}{\omega^2}\left(1 - \frac{\Omega_j^2\cos^2\theta}{\omega^2}\right)^{-1} \tag{39}$$

for $\vec{E}_1 = E_1\hat{z}$, $\vec{B}_1 = B_1\hat{y}$ polarity, where n is the index of refraction, $\epsilon(k,\omega)$ is the dialectric function for transverse electromagnetic waves, Ω_j is the local cyclotron frequency for each species j, and ω_{pj} is the plasma frequency of each species defined in Eqs. (36) and (37). All of these frequencies are conformalized quantities derived from the conformalized density and magnetic field. For example, $\epsilon(k,\omega)$ is a function of ξ through each ω_{pj}, Ω_j, and c_{sj}. Thus k is a function of ξ through Eqs. (38) and (39). We shall deal with a positron-electron plasma ($m_i = m_e$, two species) near the event horizon, which has the dispersion relations for $\vec{B}_0 \| \vec{k}$ (for both polarities),

$$\omega^2 - c^2k^2 = 2\omega_p^2 \left(1 - \frac{\Omega_e^2}{\omega^2}\right)^{-1}, \tag{40}$$

and for $\vec{B}_0 \perp \vec{k}$,

$$\omega^2 - c^2k^2 = 2\omega_p^2 \left(1 - \frac{\Omega_e^2}{\omega^2 - c_s^2k^2}\right)^{-1} \tag{41}$$

for the E_y, B_z polarity and

$$\omega^2 - c^2k^2 = 2\omega_p^2 \tag{42}$$

for the E_z, B_y polarity. The angle-dependent relation is

$$\omega^2 - c^2k^2 = 2\omega_p^2 \left(1 - \frac{\Omega_e^2 \cos^2\theta}{\omega^2} - \frac{\Omega_e^2 \sin^2\theta}{\omega^2 - c_s^2k^2}\right)^{-1} \tag{43}$$

for the E_y polarity and

$$\omega^2 - c^2k^2 = 2\omega_p^2 \left(1 - \frac{\Omega_e^2 \cos^2\theta}{\omega^2}\right)^{-1} \tag{44}$$

for the E_z polarity. Of these equations, only the E_y, B_z polarity concerns the work of this paper.

First, we elucidate the properties of the dispersion relation for a uniform plasma (uniform in the ξ space so that ω_p and Ω_e are constant in ξ space, which is not equivalent to the uniformity in real space). Equation (40) for a uniform plasma is graphed in Fig. 1(a) for the case of $\omega_p = 1$, $\Omega_e = 0.5$, and $c = 4$ in the code unit (time is normalized by ω_p^{-1}, space by the grid size Δ_ξ, and all other quantities by the combination of ω_p^{-1} and Δ_ξ). The upper branch represents the electromagnetic waves, which can propagate in vacuum, but cannot exist for frequencies lower than $\sqrt{2\omega_p^2 + \Omega_e^2}$, which is the cutoff frequency for this plasma. The lower branch represents the shear Alfvén waves, which cannot exist for a frequency greater than Ω_e, the resonant frequency for shear Alfvén waves. The graph of Eq. (41) is shown in Fig. 1(b). The upper branch remains the same as in Eq. (40). The sound speed eliminates Ω_e as a resonant frequency, though resonance is closely approached. For compressional Alfvén waves, resonance technically does not exist, though similar effects to resonance will be seen if $c_s \ll c$. Figure 2 shows the complete dispersion relation as a function of angle, where $\theta = 5°$ is very close to the shear case.

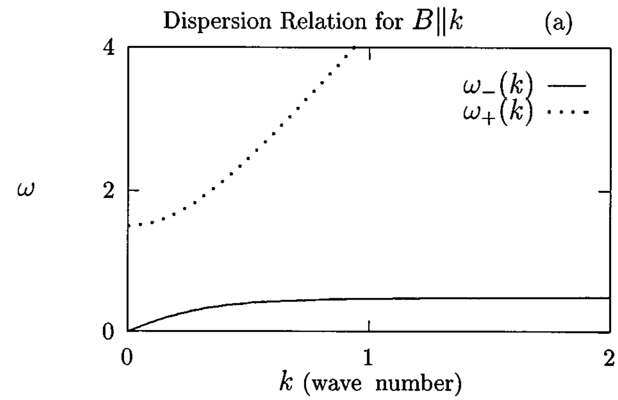

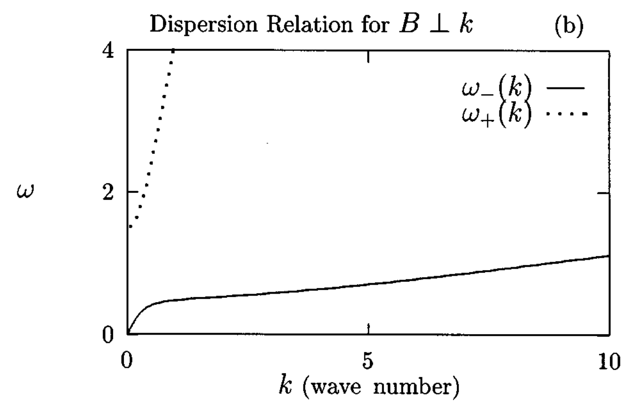

FIG. 1. Upper and lower branches of the dispersion relation for shear Alfvén waves in an electron-positron plasma appears in (a). The graph of (b) is the same, but for compressional (magnetosonic) waves. The range of k in this second graph has been extended to show the effect of the compressional relation.

IV. CUTOFF AND RESONANCE

There are two major types of waves we shall consider, which are the two branches of the electron-positron plasma. The upper branch describes the electromagnetic waves, which are capable of propagating in vacuum. The lower branch is the set of Alfvén waves, the shear Alfvén waves and compressional Alfvén waves.

As a wave propagates from one region to another, it may enter a region in which it is disallowed, as ω_p becomes larger than ω for the electromagnetic waves or as Ω_e becomes too small for a given ω of the shear Alfvén waves. At the point of transition from an allowed to a precluded region, a cutoff or resonance occurs. A cutoff occurs when the index of refraction (ck/ω) goes to zero. A resonance occurs when the index of refraction goes to infinity. The presence of a strong Schwarzschild background affects, through the spatial-coordinate-dependent lapse function, how and whether or not a cutoff or resonance occurs for the plasma waves near the event horizon.

A. Particle simulation code

We developed a $1\frac{2}{2}$ particle-in-cell PIC code [11] appropriate for simulating self-consistently electromagnetic plasma phenomena near the event horizon. In Ref. [11], general discussion of the PIC code in a general metric is given.

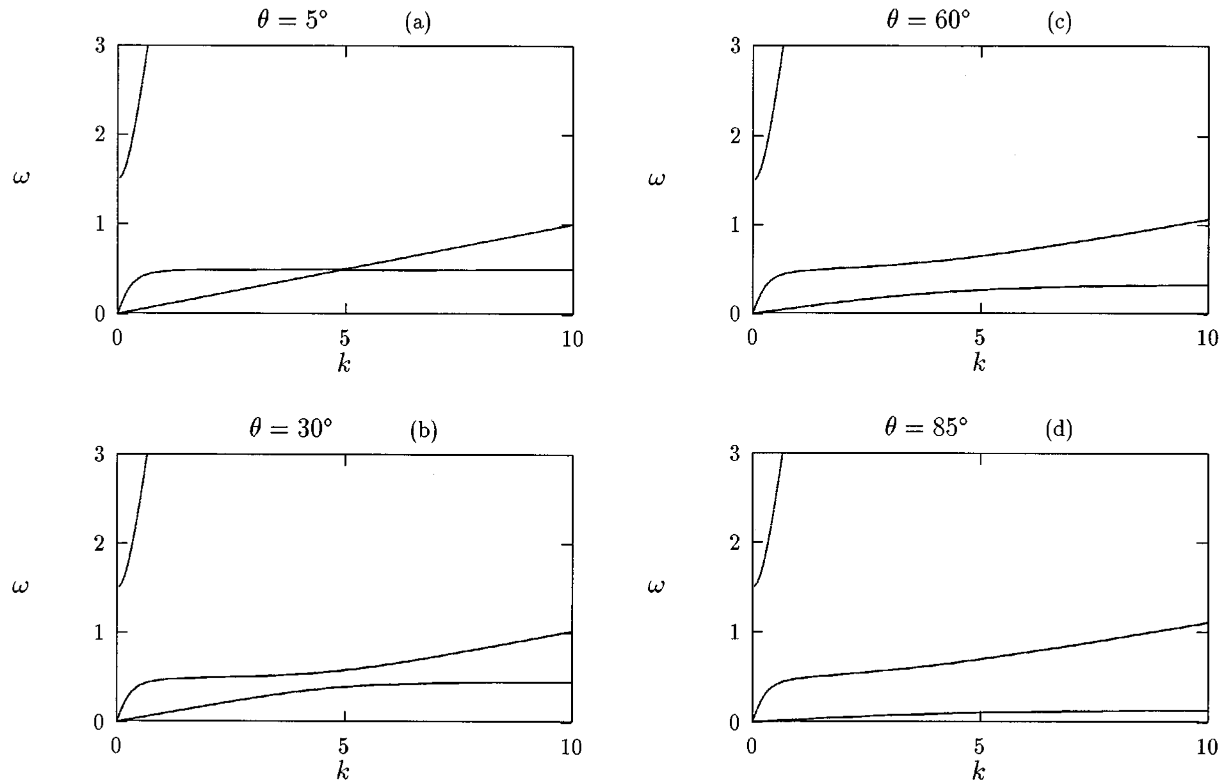

FIG. 2. Dispersion relation for an electron-positron plasma, Eq. (43), for four cases of the angle between $\vec{B}_0$ and $\vec{k}$. The upper branch is the same in each case. The lower two branches are the magnetosonic and the sound waves. The temperature of the plasma for these graphs is higher than for those in Fig. 1, increasing the sound speed and making the qualitative behavior of the lower two branches more obvious.

We also employ the absorbing boundary conditions at either end of the box [12]. The PIC code is used instead of a fluid code to study the high-frequency phenomena in a plasma and to be able to model some of the instabilities which can occur. The main feature of a fluid model is that there is one particular velocity associated with any given point. While this is a useful model that allows modeling of slow large-scale phenomena, it excludes the possibility that there can be several different particles associated with a given point, each with its own velocity. Thus a fluid model cannot be used to study the physics of particle acceleration, for example, which is one of the most interesting expected physics around the event horizon. One of the main objectives of this paper is to study high-frequency EM spectroscopy in which mode conversions between different modes of the plasma, such as between Alfvén waves and electromagnetic waves and their interaction with particles.

That the code is $1\frac{2}{2}$ dimensional means that quantities can be functions of only one spatial parameter. There is only the one spatial degree of freedom in which particles and waves can propagate. It also means that the electromagnetic field vectors can exist in any direction and that the momentum of the particles can exist in any direction (i.e., particles are said to be planar). Typical runs are done with about 20 000 particles, half electrons and half positrons, in 2048 cells in the one-dimensional grid, and the size of a cell is about two-thirds of a Debye length. The electron plasma frequency is defined as 1, and time is measured in inverse plasma frequencies. The time step is typically $0.1\omega_p^{-1}$, where ω_p is the average (in ξ-space) plasma frequency.

There are four major sets of results to be presented here: (i) a demonstration of the resonant behavior of Alfvén waves approaching the event horizon, (ii) the cutoff and reflection of an electromagnetic wave initially propagating away from the hole, (iii) an analysis of the mode conversion of Alfvén waves into EM waves in a rapidly varying background plasma, and (iv) particle acceleration associated with this mode conversion. In all of these cases, we are graphing parameters versus ξ, which is the grip spacing of the cells. Refer to Eq. (23) to recall the relation between the distance to the event horizon and ξ. The numerical value assigned to the Schwarzschild radius is $R_S = 16\,096$ (in a unit of the grid size Δ_ξ) for the first two sets of results and $R_S = 220$ for the mode conversion example. These values are chosen such that the phenomena to be observed fits within the framework of the code and do not readily translate to astronomical scales.

B. Resonance

The presence of the strong Schwarzschild background can make a resonance appear when it otherwise would not have. In the type of plasma we are considering, a resonance will only occur for a shear Alfvén wave, when the conformalized cyclotron frequency decreases below the frequency of the wave. Let us assume that $B_0 = \text{const}$ with respect to position. Then the local conformalized cyclotron frequency varies as $\Omega_{e\xi} = \alpha(\xi) e B_0 / mc$. Any shear Alfvén wave that is approaching the black hole under these conditions will reach a resonance point, since the conformalized cyclotron fre-

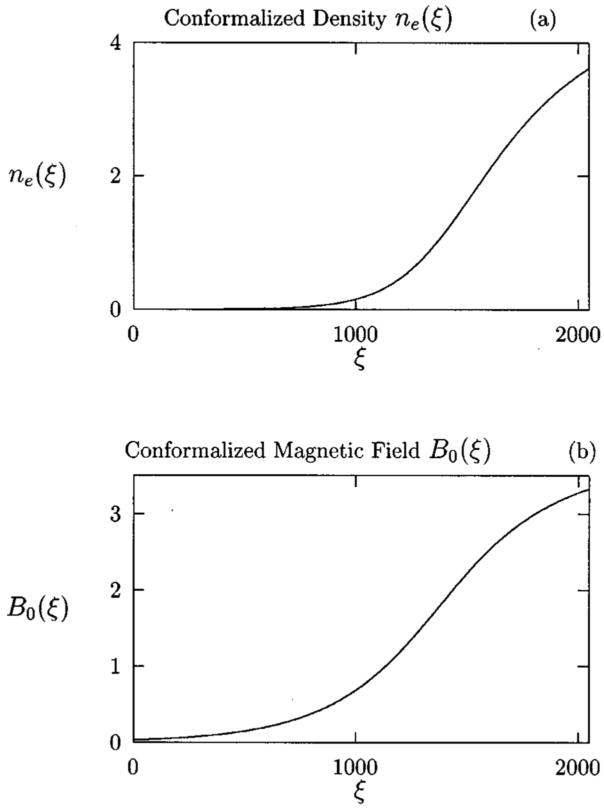

FIG. 3. Conformalized density profile (a) and conformalized magnetic field (b) of a plasma measured in ξ space. The profiles are constant in r space. The Schwarzschild radius is 16 096 units. The grid has been rescaled by a factor of 100, so that $r=2R_S$ corresponds to $\xi\approx 1700$, $r=R_S+1000$ maps to $\xi\approx 1100$, and $\xi=400$ is scarcely 12 units away from the event horizon as measured in r space.

quency approaches zero at the event horizon. This resonance point would not occur without the presence of the background Schwarzschild metric.

The graph of Fig. (3a) is a graph of the effective density $n_{e0\xi}(\xi)$ vs ξ. This is a conformalized quantity, and the particle density as measured versus r is a constant. Similarly, Fig. 3(b), is a graph of $B_{0\xi}(\xi)$ vs ξ. This, too, is a conformalized quantity: The physical value of B_0 is a constant with respect to position. In order to obtain physical (i.e., nonconformalized) quantities, we should convert these conformalized quantities over through Eqs. (27)–(30) and (23). In this background, we look at a shear Alfvén wave in Fig. 4, progressing from a position at $\xi=1600$ to a resonant point at $\xi=1084$. The graphs are taken at time intervals $100.0\omega_p^{-1}$ apart. If we plot (physical) magnetic fields B_z in (physical) r coordinate, Fig. 4 would show a larger amplitude with a larger wave number toward the left (the event horizon).

C. Cutoff

Another test case considers an electromagnetic wave of the upper branch propagating in a region where the background number density, $n_0(r)=\text{const}$. This is intended to be purely hypothetical case to aid theoretical discussion and is not intended to suggest that such a constant background density would likely exist in the environment being discussed near the event horizon. In this case, the plasma frequency varies as $\omega_{p\xi}=\alpha(\xi)\sqrt{4\pi n_0 e^2/m}$. The lapse function α increases monotonically with respect to both r and ξ, varying from zero to one. There can be an electromagnetic wave close to the black hole in this scenario of some frequency less than $\sqrt{4\pi n_0 e^2/m}$, which is propagating away from the hole. At the point when $\omega_{p\xi}>\omega$ becomes true, the wave hits a cutoff point, and reflects back towards the hole. A different way of looking at this phenomenon is that the wave heading away from the hole is getting redshifted to a lower and lower frequency, until its frequency is less than the local plasma frequency as measured in nonconformalized coordinates. This phenomenon can occur regardless of the state of the background magnetic field.

Figure 5 shows a wave of the upper branch traveling from about $\xi=400$ to a cutoff point at $\xi=1100$ and reflecting. The conditions for this run are the same as for the previous one, except that we have generated an electromagnetic pulse traveling outward rather than an Alfvén pulse traveling inward. We have graphed $E_{y\xi}$ vs ξ, the conformalized transverse electric field. In this conformalized space, the pulse sees the density contour graphed in Fig. (3a), which quickly raises the effective plasma frequency starting at around $\xi=1000$, until the effective plasma frequency is too high to allow the wave to propagate farther in that direction. The time interval between successive frames is $100\omega_p^{-1}$.

D. Mode conversion

In the more generalized case, a magnetic field of any shape will have a conformalized counterpart which approaches zero at the event horizon, and any density profile will have the same. If we are looking at a background of either of these variables that is very high close to the event horizon and decreases with the distance from it (assuming that α approaches zero faster than the magnetic field goes to infinity and that α^2 approaches zero faster than the density approaches infinity), we will see a region in which these conformalized background quantities have a maximum and approach zero at the event horizon and at infinity. For electromagnetic waves, this means a region in the atmosphere which reflects low-frequency waves both back toward the horizon and back away from the hole. For Alfvén waves, this means there is a region near the horizon, but not touching it, where such waves dominate. Beyond this region, no significant Alfvén waves could propagate.

In this section, we will consider a varying background magnetic field and a varying background density. These backgrounds are the nonconformalized fields, whose relation to the conformalized fields is expressed in Eqs. (36) and (37). The density $n_e(r)$ is assumed to vary as $n_e(r)\propto e^{-(r-R_S)/h}$ and the background magnetic field varies as $\vec{B}_0(r)\propto e^{-(r-R_S)/2h}$, where h is an arbitrary scale height. In the particular cases considered, $R_S=220$ and $h=150$. The exponential decay of these parameters as one gets far from the hole means that there is no *qualitative* difference between the ''slab'' metric approximation we introduced in Sec. II A and the original spherical metric: Mode conversion and particle acceleration would still occur with the spherical boundary conditions, but the specific locations of resonance

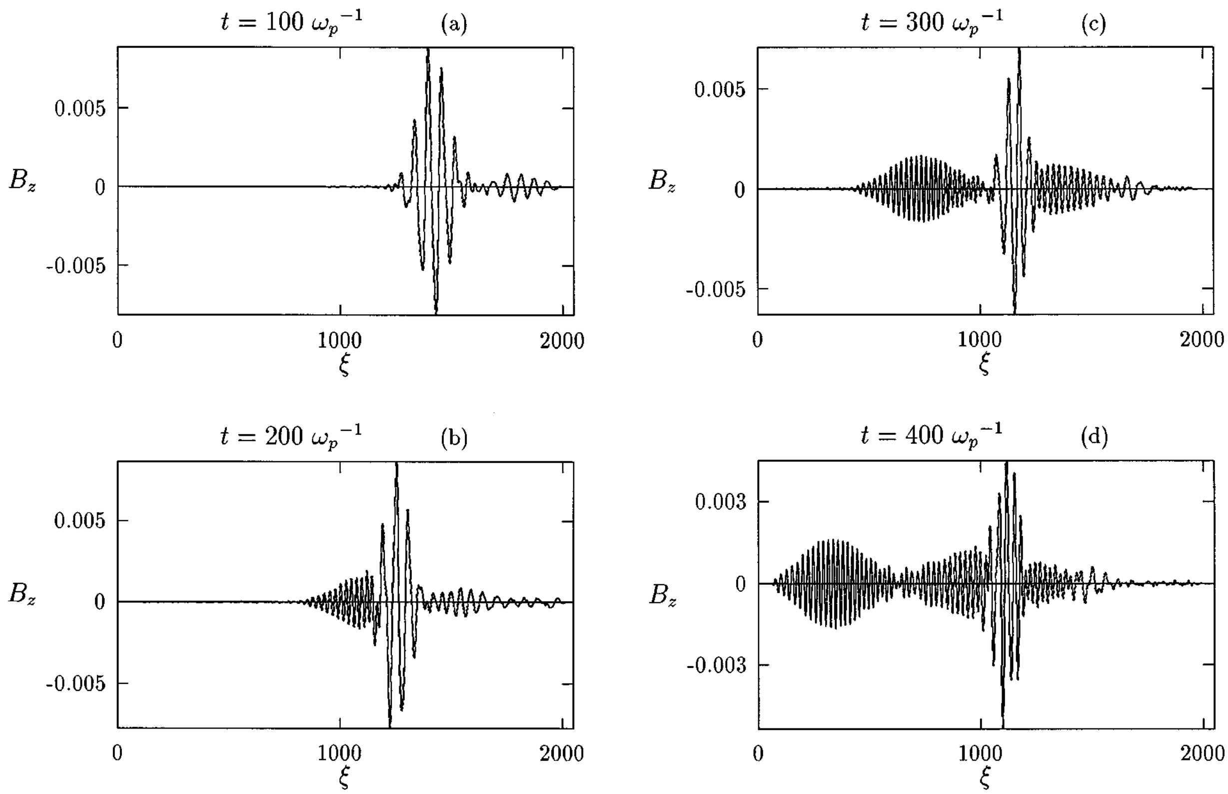

FIG. 4. An Alfvén pulse travels inward towards the black hole, starting from the right side of the grid. There is a resonance point at $\xi \approx 1084$, beyond which the pulse does not propagate. The resonance point exists only because of the strong Schwarzschild metric.

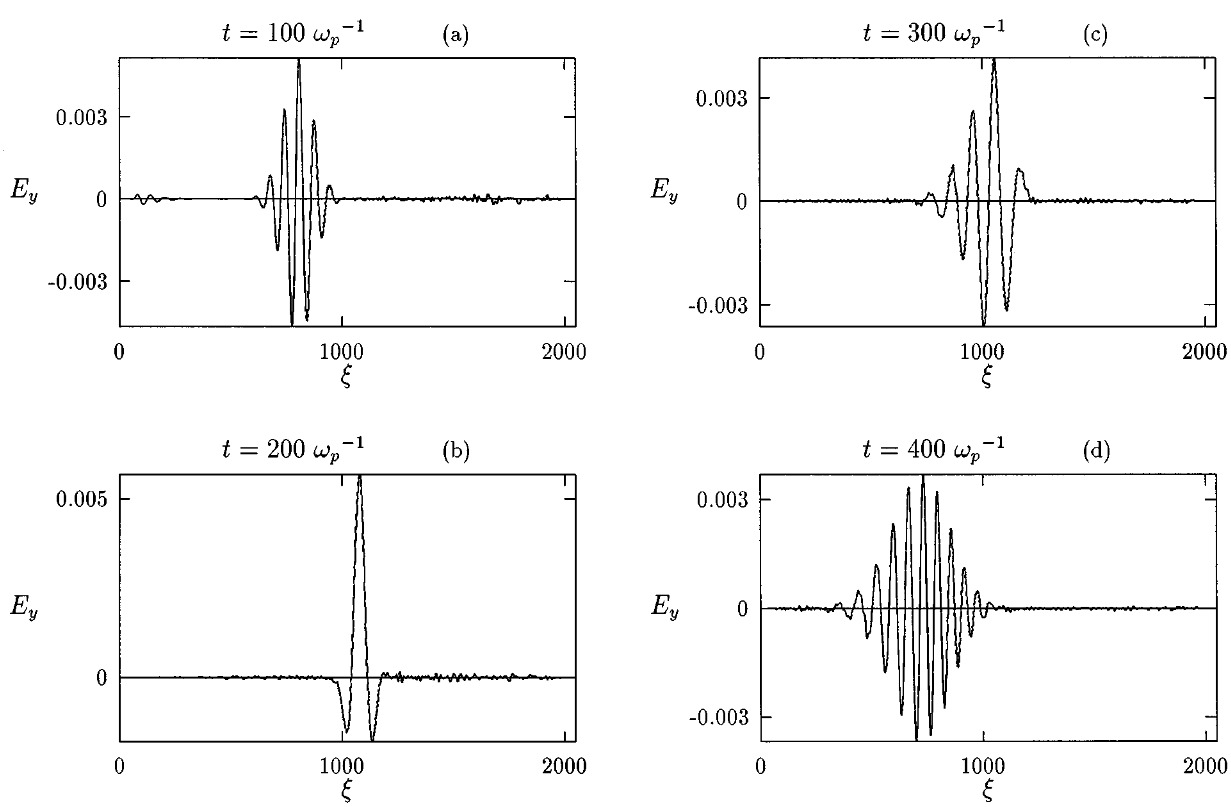

FIG. 5. Progress of an electromagnetic wave propagating away from a black hole in a region of constant background particle density. The wave starts on the left side of the grid, where the conformalized density is low, propagates to the right, away from the hole, hits a cutoff point at $\xi \approx 1100$ in (b), and is reflected back towards the hole. The cutoff point would not exist without the general relativistic effect of the hole.

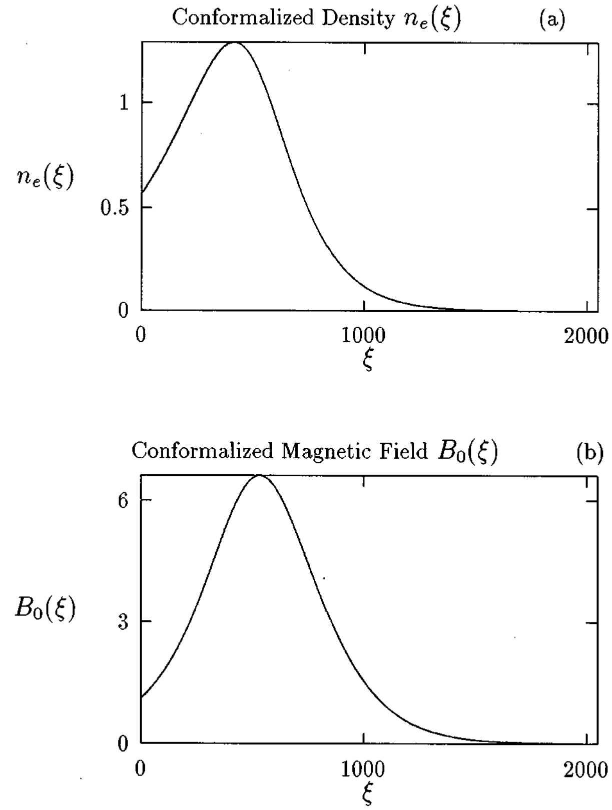

FIG. 6. Background number density (a) and background magnetic field (b) for the mode conversion simulation. The scale height (in r) is 150 units, and the Schwarzschild radius is 220 units. $\xi=400$ is about 40 units from the event horizon, and $\xi=1000$ is about 700 units from the horizon.

and cutoff points would be different. The properties of EM wave propagation are characterized by $n^2=\epsilon(k,\omega)$, as shown in Eq. (38). In our present formulation, the frequency ω is constant (see Sec. II B). Thus, when the dielectric function ϵ is nonuniform in ξ through the lapse function α (or through background plasma parameters), the dispersion relation makes the wave number k (i.e., k_ξ) nonuniform in ξ. Figures 6(a) and 6(b) show the conformalized density profile and background magnetic field. There is an Aflvén pulse that will start at $\xi=416$ and propagate outward (in the positive ξ direction). The graph in Fig. 7 is a plot of k^2 vs ξ, for a given constant frequency ω, assuming the $\theta=0$ shear Alfvén wave dispersion relation with $n>1$. It is used to analyze (within the limits of WKB) the behavior of the pulse. There is a predicted resonance of the pulse at $\xi\approx1019$ for the shear case. The compressional Alfvén case would be very similar to this, except that full resonance is not quite reached. Beyond this point is a region ($\xi\approx1020-1049$) where no wave of this frequency should propagate. At $\xi\approx1050$, there is a cutoff point, beyond which the upper branch mode may propagate with $n<1$, at the same frequency as the Alfvén mode. An analysis of wave propagation through this mixed resonance or cutoff point has been done by Budden [13] and is known as a "Budden turning point."

The WKB wave equation here is

$$\Psi''+k^2(\xi)\Psi=0, \tag{45}$$

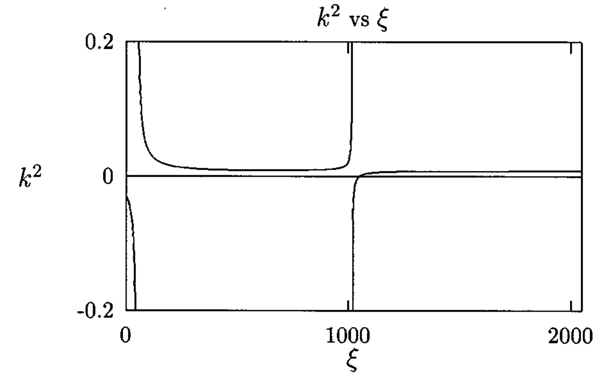

FIG. 7. k^2 vs ξ. This plot determines where resonance and cutoff occur for the mode conversion case of Sec. IV D. k^2 is proportional to the square of the index of refraction: As $k^2\rightarrow\infty$, resonance is approached. Cutoff occurs where k^2 changes sign. At $\xi\approx1020$, there is a resonance-cutoff pair (a Budden turning point) with a separation small enough to allow transmission from the Alfvén region ($\xi<1020$) to the EM region ($\xi>1049$).

and $k^2(\xi)$ can be approximated as

$$k^2(\xi)=\frac{\beta}{\xi}+\frac{\beta^2}{\eta^2}, \tag{46}$$

where $\beta^2/\eta^2=k_\infty^2$, $\eta=|\Delta x k_\infty|$, Δx is the distance between the resonance and cutoff of the turning point, and k_∞ is the wave number far from the turning point. For the Alfvén wave near the event horizon to leak out of this plasma and mode convert itself into a vacuum (or low-density plasma) EM wave, $\eta=|k_\infty\Delta x|$ should not be much greater than unity. When η is much greater than unity, Budden turning point acts as a perfect wave absorbing point, an important property of the Budden turning point. For a sufficient amount of EM waves to propagate out of the hole, it is necessary to rapidly change the stratification of the atmosphere near the hole. From this information, Budden predicts that the transmission coefficient will be

$$|T|=e^{-\pi\eta/2}, \tag{47}$$

where $|T|$ is the coefficient of the absolute value of the amplitude (not the square of the amplitude). The reflection coefficient in this case is $|R|=0$.

The run in which this is modeled starts with a shear Alfvén pulse on the left side of the grid, centered at $\xi=416$. Figures 8 and 9 show the progress of the pulse at $100.0\omega_p^{-1}$ intervals. The condition for an Alfvén pulse is $v_{ph}<c$, which can also be written as

$$\frac{|E|}{|B|}=\frac{\omega}{kc}=\left(1-\frac{2\omega_p^2}{\omega^2(1-\Omega_e^2/\omega^2)}\right)^{-1/2}<1. \tag{48}$$

At $t=0.0\omega_p^{-1}$, $|E|<|B|$, confirming that the code is modeling an Alfvén wave in this regime. The condition for the upper branch electromagnetic wave is the converse: $|E|>|B|$. Measuring the relative magnitudes of E and B of the pulse at $t=300.0\omega_p^{-1}$ that has passed the turning point, the

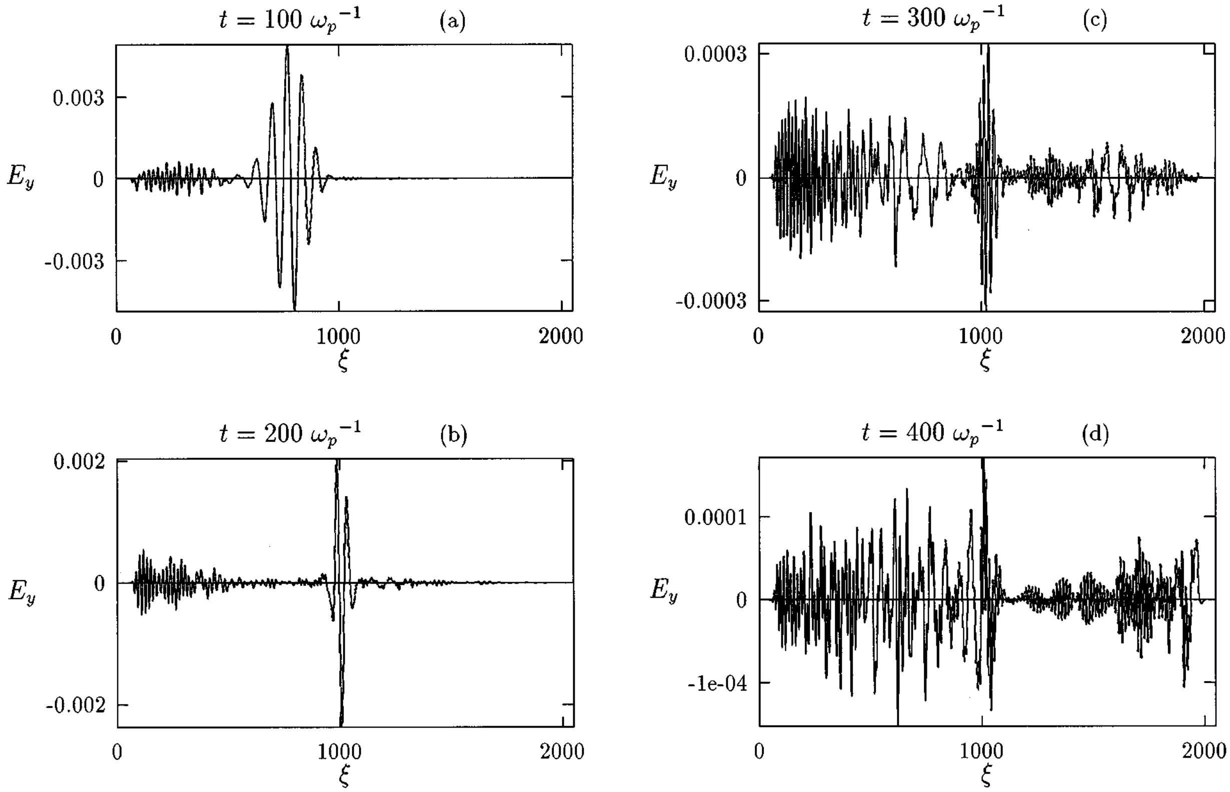

FIG. 8. An Alfvén pulse starts at the left side of the grid in (a) and hits the resonance point at $\xi \approx 1019$ in (b). An electromagnetic pulse is visible at $\xi \approx 1600$ in (c), having been transmitted past the turning point. In (d), the last vestiges of the transmitted pulse are visible at the far right of the grid, and the rest of the initial pulse remains at the resonance point. These graphs show the E_y component of the waves.

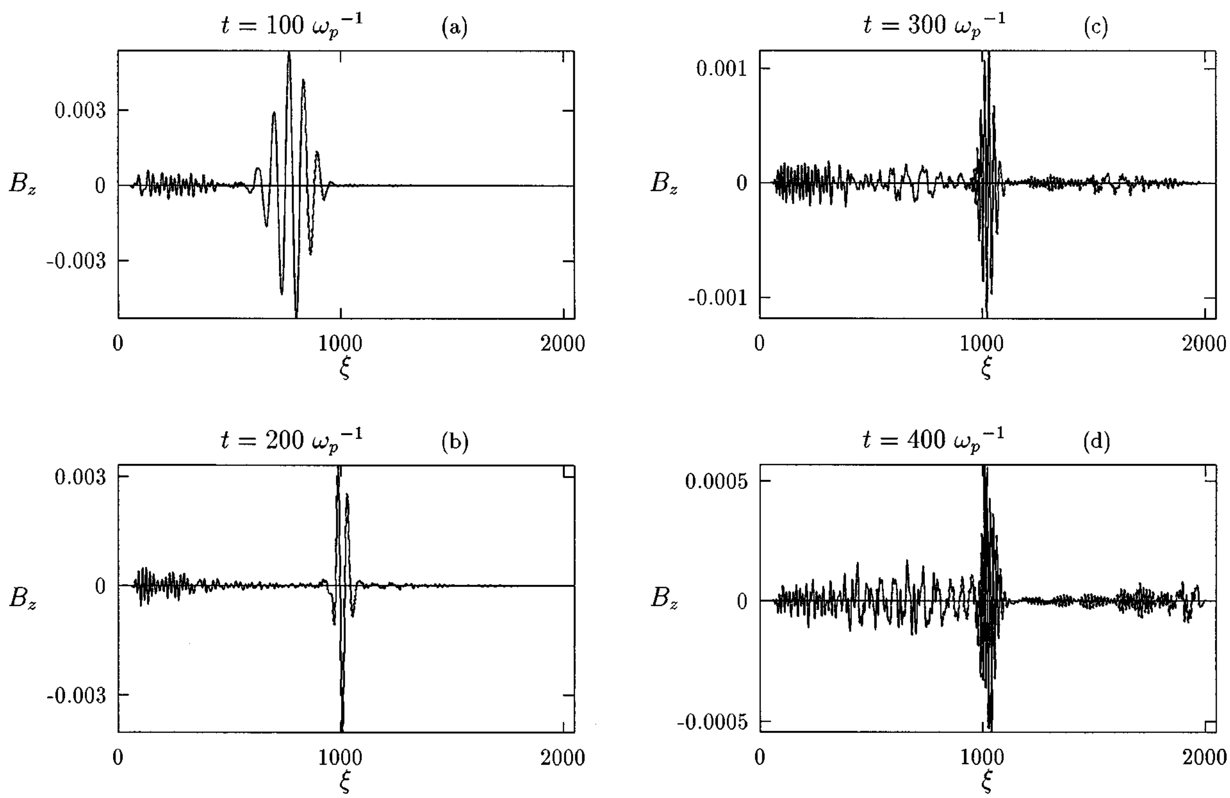

FIG. 9. As in Fig. 8, except showing the B_z component of the waves. The pulse starts in the shear Alfvén mode in (a), hits resonance at $\xi \approx 1019$ in (b), and an EM pulse is transmitted past the turning point and is visible at $\xi \approx 1600$ in (c), while the rest of the wave remains and is absorbed at the turning point in (d).

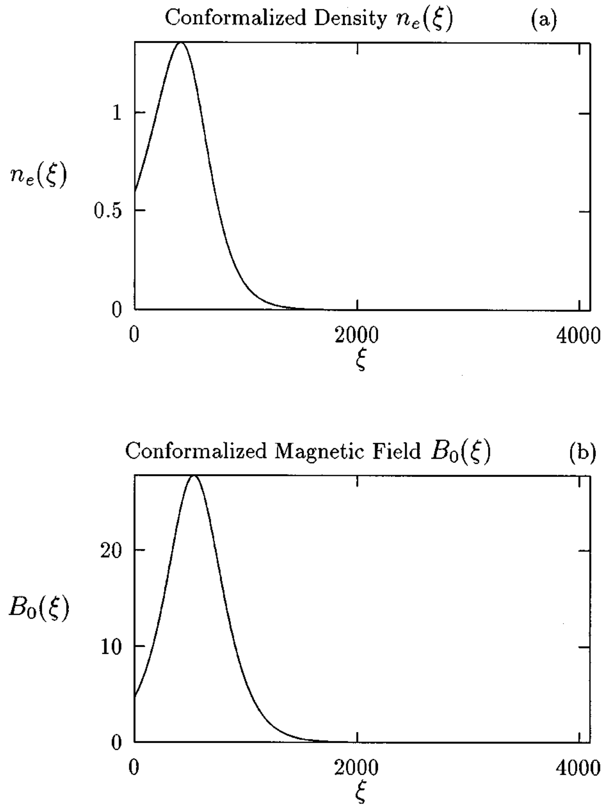

FIG. 10. Background number density (a) and background magnetic field (b) for the particle acceleration simulation. The initial pulse starts as $\xi = 416$ and progresses to the right, away from the event horizon. The scale of the grid is the same as for the mode conversion simulation, but it has been doubled in size to show progress still further from the horizon.

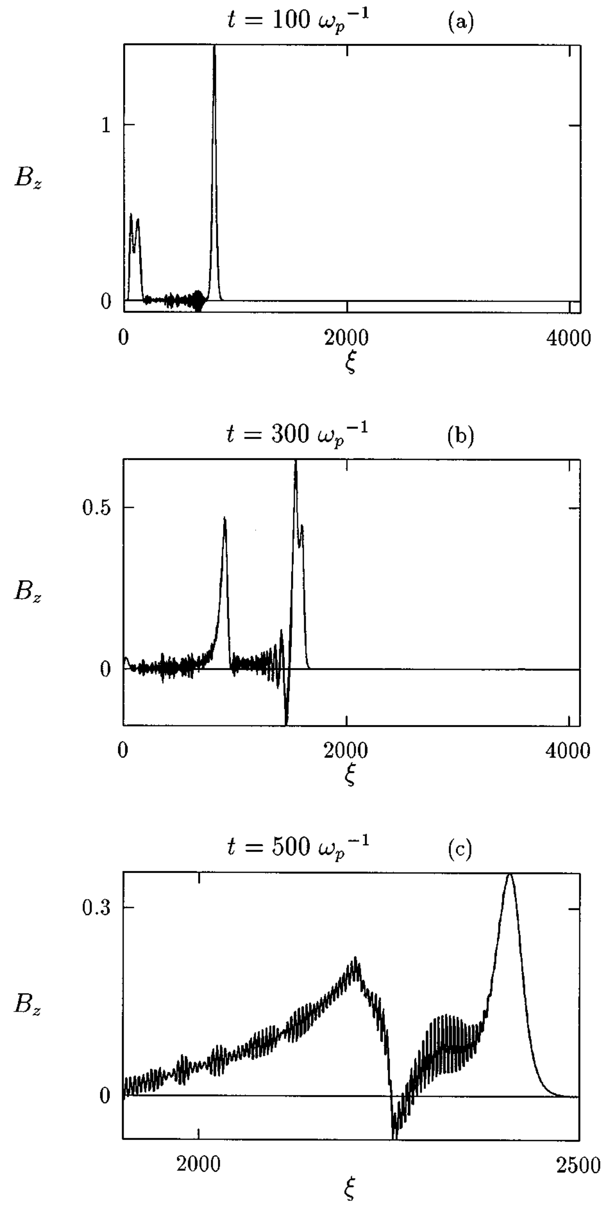

FIG. 11. Progress of the magnetic field for the particle acceleration simulation, graphed in $200\omega_p^{-1}$ intervals, starting at $t = 100\omega_p^{-1}$. The solitary wave splits into shear Alfvén and EM modes in (b) at $\xi \approx 1600$. The right peak is in the EM mode, and the left peak is in the Alfvén mode.

result is $|E|/|B| \approx 1$. Since $\omega_p \ll \omega$ and $\Omega_e \ll \omega$ in this region of $\xi > 1100$, the $2\omega_p^2/[\omega^2(1-\Omega_e^2/\omega^2)]$ term of the dispersion relation is very small, which implies that $|E|/|B| \approx \Omega_e \ll \omega$ also implies that the Alfvén branch does not exist here at this frequency. Therefore this run indeed models mode conversion from an Alfvén near the hole to an electromagnetic wave away form the hole.

In this particular case, Budden predicts that $|T| \approx 0.0159$ and that the rest of the wave is absorbed by the resonance (no reflection coefficient). The run shows no reflection, as expected, and a necessarily rough comparison between the amplitude of the incoming wave and the outgoing wave indicates a measurable transmission of $|T| \approx 0.01$, very close to the predicted value.

This mechanism for mode conversion allows the observation of possible signatures of Alfvén mode events near a black hole, by permitting the emission of a corresponding electromagnetic pulse, which may propagate into a vacuum, i.e., interstellar space, and eventually to our eye. Behavior near a suspected black hole can be modeled via our conformalism, and the model can make a prediction about possible observable behavior far from the hole.

E. Bursty acceleration out of a black hole atmosphere

Particle acceleration possibly triggered from a violent motion of matter near the event horizon may be simulated with this computational model. Without going into specifics (to be published elsewhere), we can imagine a situation where accreting matter [14] interacts with the magnetic field of the black hole magnetosphere [15] and this accreting mass motion can trigger Alfvén wave pulse(s). This situation is a bit similar to that considered for (compressional) Alfvén wave acceleration around a neutron star [16]. The initial setup is similar to the mode conversion discussed in the previous subsection. The main difference is that the Alfvén pulse is a solitary wave, with the typical $\mathrm{sech}^2(\xi - v_{\mathrm{gr}}t)$ profile. (It is imperfectly generated, and so part of the initial pulse travels toward the horizon on the left side of the grid and bounces of the reflective boundary condition there. This is because the frequency of this ''wave'' is broadbanded and instantaneous

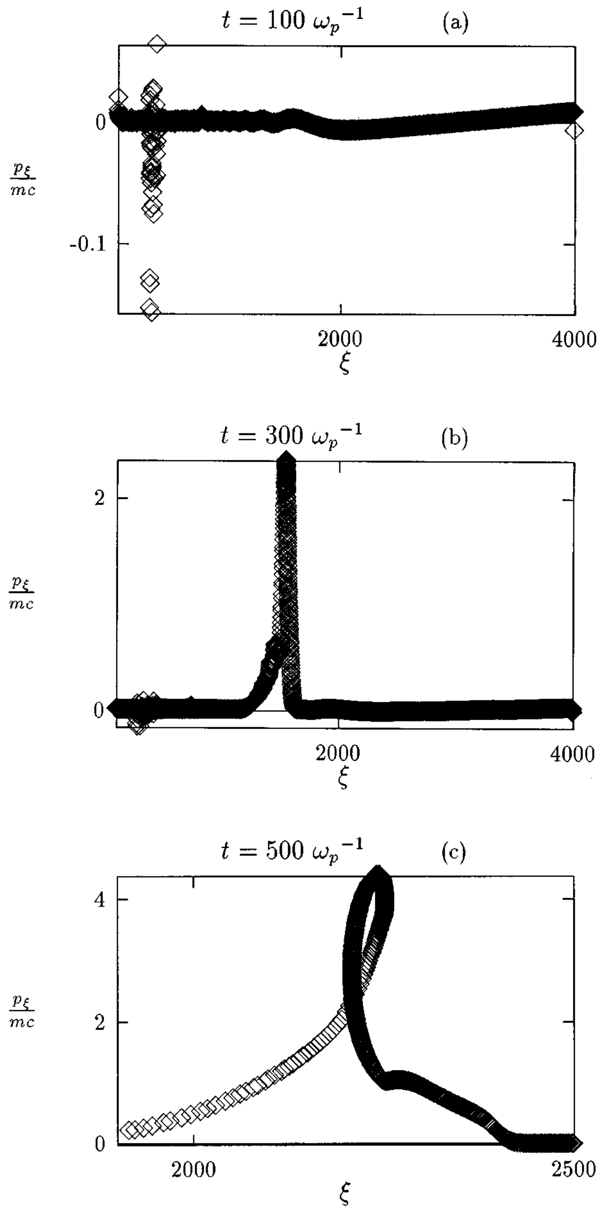

FIG. 12. The ξ component of the momentum of the electrons is graphed in $200\omega_p^{-1}$ intervals, starting at $t=100\omega_p^{-1}$. The acceleration of a significant fraction of the plasma is evident. The ''looping'' of the phase space in the later graphs indicates particle trapping, as the particles oscillate within their accelerating potential well.

wave turn-on is difficult. The physics of interest is elsewhere on the grid, and the secondary pulse does not change the qualitative results.) Figure 10 shows the scaling of the conformalized background parameters, and Figs. 11 and 12 show the progress of the initial pulse and the attendant particle acceleration. Figure 11 graphs the transverse magnetic field and shows the pulse propagating to the right, to eventually encounter a broadband resonance near the middle of the grid, from $\xi \approx 1500$ to $\xi \approx 2500$ (the pulse has a large bandwidth, and individual frequencies of the pulse hit resonance over a large range of positions). To the left of this resonance, the solitary wave is a shear Alfvén wave. To the right, the pulse penetrates the resonance and becomes an electromagnetic pulse, the wake of which has trapped some particles and has accelerated them to relativistic velocities. In Fig. 11(b), the pulse can be seen splitting (a distinctive double peak at $\xi \approx 1500$, the left half of the peak is the Alfvén mode, where $|B| > |E|$, and the right half is the EM mode, where $|E| \approx |B|$. Figure 12 shows the P_ξ vs ξ phase space. As the pulse propagates away from the hole, the momentum of the particles trapped with it increase significantly, reaching relativistic speeds. The mechanism for such solitary wave acceleration is discussed by Rau *et al.* [17].

V. CONCLUSION

We have developed a conformalism for general relativistic plasma physics that greatly simplifies the dynamical study in a strong Schwarzschild background and a simulation model based on this formalism. A simple transformation turns the Maxwell's equations of Thorne, Price, and McDonald into ''flat'' equations. Our results indicate that a strong gravitational field effect introduces stratified ''nonuniformity'' effects in plasma parameters and that, in the plasma near the event horizon, induce cutoff and resonant effects independently of any contour of density and magnetic field. In addition, we demonstrated that internal magnetic modes can be conceivably converted into observable electromagnetic emissions. As the plasma and its motion are expected to be quite violent near the event horizon, such violent plasma dynamics is expected to give rise to large amplitude. Alfvén waves and magneto hydrodynamics (MHD) instabilities. The large amount of energy contained in this low-frequency branch of the plasma wave dispersion relation, however, cannot by itself be convected out of the event horizon, barring the usual thermal processes, unless the above-mentioned mode-conversion process occurs. Thus this mode-conversion process constitutes an important path of the energy as well as the observational window into signatures important to the spectroscopy of a black hole. The investigation into mode conversion will continue, as there is good reason to believe that such behavior can lead to visible emissions and cosmic ray bursts that would be observable evidence of the behavior of a black hole near the event horizon.

ACKNOWLEDGMENTS

This work was supported in part by the U.S. DOE and NSF.

[1] Y. Tanaka, in *Proceedings of the 23rd ESLAB Symposium—X-ray Astronomy*, Paris, 1989, edited by J. B. Battrick *et al.* (European Space Agency, Paris, 1989), p. 3.
[2] A. P. Cowley *et al.*, Astrophys. J. **272**, 118 (1983).
[3] K. Holcomb and T. Tajima, Phys. Rev. D **40**, 3809 (1989).
[4] N. Frankel *et al.*, Phys. Rev. D **48**, 5655 (1993).
[5] G. Tarkenton and T. Tajima (unpublished).

[6] G. Tarkenton, Ph.D. dissertation, University of Texas at Austin, 1996.
[7] C. Misner, K. Thorne, and J. Wheeler, *Gravitation* (Freeman, New York, 1973).
[8] M. A. Nowak and R. V. Wagoner, Astrophys. J. **393**, 697 (1992).
[9] D. A. MacDonald and K. Thorne, Mon. Not. R. Astron. Soc. **198**, 345 (1982).
[10] K. S. Thorne *et al.*, *Black Holes: The Membrane Paradigm* (Yale University Press, New Haven, CT, 1986).
[11] T. Tajima, *Computational Plasma Physics* (Addison-Wesley, Reading, MA, 1989).
[12] T. Tajima and Y. C. Lee, J. Comput. Phys. **42**, 406 (1981).
[13] K. G. Budden, *Radio Waves in the Ionosphere* (Cambridge University Press, Cambridge, England, 1961).
[14] O. M. Blaes, Mon. Not. R. Astron. Soc. **227**, 975 (1987).
[15] C. M. Mobarry and R. V. E. Lovelace, Astrophys. J. **309**, 455 (1986).
[16] K. Holcomb and T. Tajima, Astrophys. J. **378**, 682 (1991).
[17] B. Rau, T. Tajima, and H. Hojo (unpublished).